Draft January 5, 2007

MOJAVE: Monitoring of Jets in AGN with VLBA Experiments. III. Deep VLA Images at 1.4 GHz

N. J. Cooper

Department of Physics, Purdue University, 525 Northwestern Avenue, West Lafayette, IN 47907

ncooper@physics.purdue.edu

M. L. Lister

Department of Physics, Purdue University, 525 Northwestern Avenue, West Lafayette, IN 47907

mlister@physics.purdue.edu

M. D. Kochanczyk

Department of Physics, University of Texas at Austin, 1 University Station C1600, Austin, TX 78712

martin@physics.utexas.edu

ABSTRACT

The MOJAVE blazar sample consists of the 133 brightest, most compact AGN in the northern sky, and is selected on the basis of 15 GHz VLBA flux density. Since 1994 we have been gathering VLBA data on the sample to measure superluminal jet speeds and to better understand the parsec−scale kinematics of AGN jets. We have obtained 1.4 GHz VLA−A configuration data on 57 of these sources to investigate whether the extended luminosity of blazars is correlated with parsec−scale jet speed, and also to determine what other parsec−scale properties are related to extended morphology, such as optical emission line strength and gamma−ray emission. We present images and measurements of the kiloparsec scale emission from the VLA data, which will be used in subsequent statistical studies of the MOJAVE sample.

Subject headings: galaxies : active — galaxies : jets — quasars : general — radio continuum : galaxies — BL Lacertae objects : general —

1. Introduction

Blazars are an extreme class of radio source that represent only a small percentage of active galactic nuclei (AGN), yet dominate the sky at high energies. They are characterized by highly relativistic jets that are oriented toward us with a very small angle of incidence. This often results in apparent superluminal jet motions that are caused by a Doppler compression in the apparent time duration of signals from the source. This creates an ideal set of circumstances for studying the kinematics of jets, since many decades of evolution are often compressed into much shorter timescales. MOJAVE (Monitoring of Jets in Active galactic nuclei with VLBA Experiments) is a long term program that seeks to better understand the physics of AGN on the parsec−scale via regularly−spaced, high resolution VLBA observations (Kellermann et al. 1998, 2004; Lister & Homan 2005). The MOJAVE sample contains 133 sources satisfying the criteria,

- Declination $> -20^\circ$
- Galactic latitude $|b| > 2.5^\circ$
- VLBA 2 cm correlated flux density exceeding 1.5 Jy (2 Jy for declination south of Dec $= 0^\circ$) at any epoch between 1994 and 2003.

By selecting on the basis of compact flux density at a short wavelength, the sample favors highly beamed relativistic jets (i.e., blazars). This makes it well suited for quantifying the strong selection effects associated with blazar samples (Lister & Marscher 1997).

An important goal of the MOJAVE program is to gain a better understanding of how AGN jets evolve from parsec to kiloparsec−scales. Parsec−scale jet speed information on the sample is nearly complete (Lister et al., in preparation), and a distinct upper envelope is seen in a plot of maximum observed jet speed versus parsec−scale jet luminosity (Cohen et al. 2007). The shape of this envelope is suggestive of an intrinsic correlation between jet speed and synchrotron luminosity. Early hydrodynamic models (Blandford & Rees 1974) predict

such behavior, and if verified, would prove useful for constraining more recent numerical models of jet production that include full magneto-hydrodynamic (MHD) and general relativistic (GR) effects (e.g., Kato, Mineshige & Shibata 2004).

The interpretation of the envelope is complicated by the fact that the apparent luminosity of blazar jets is strongly affected by the bulk Doppler factor (δ), of the flow. The latter quantity is dependent on the Lorentz factor and viewing angle of the jet, which also affect the apparent speed. An alternate means of testing the intrinsic speed/luminosity correlation is to compare the apparent jet speeds with extended (radio lobe) emission on kiloparsec−scales. The extended emission is not appreciably beamed and is well-correlated with the total jet power (Giovannini et al. 1988).

Several extended flux density surveys that include blazars have been carried out with the VLA (e.g., Antonucci & Ulvestad 1985; Murphy, Browne & Perley 1993; Cassaro 1999; Rector, & Stocke 2001). However, none of these samples were as large or complete as MOJAVE, and they lacked parsec−scale kinematic information. In order to measure the relatively weak extended radio emission in the presence of a strong, highly beamed blazar core component, images with good angular resolution and very high dynamic range are necessary. Although better resolution can be achieved at higher observing frequencies, the extended emission becomes fainter because of the steep spectral index. We have therefore sought to obtain deep VLA−A configuration images of the entire MOJAVE sample at 1.4 GHz, which represents a reasonable compromise between angular resolution and sensitivity to extended emission. Here we present images of 57 MOJAVE sources; data on the remaining objects (from the VLA archive and other observations) will be presented in an upcoming publication.

2. Observations

The observations were made with the VLA in the A configuration, which yields a typical restoring beam of 1.5" (FWHM), at a wavelength of 20 cm. To minimize the possible effects of radio interference, and to improve the dynamic range, the data were recorded in spectral line mode, with 8 channels per IF. Right− and left−hand circular polarization data at 1.36 GHz and 1.44 GHz were each assigned to one of four IFs, each having bandwidth of 25 MHz. The observations took place during filler time on six separate dates between 2004 September 19 and 2004 November 24 (Table 1). To maximize *(u,v)* coverage, two scans of approximately five−minutes duration, separated in hour angle, were made on each source. This yielded typical r.m.s. noise levels of 0.14 mJy beam^{-1} and dynamic ranges of $\sim 15000 : 1$. Two sources, 0059+581 and 0109+224, had less than 10 minutes integration

time, due to scheduling constraints. Data on three high declination sources (0016+731, 1150+812, 1459+718) were not analyzed due to poor *(u,v)* coverage.

Calibration of the data was performed in AIPS [1],and futher imaging and self-calibration steps were carried out with Difmap [2]. For each source, the flux density of the core component was determined by fitting a Gaussian component to the visibility data. The total flux density was determined by summing the flux density within a box fitted around the extent of the source. The r.m.s. noise was measured in a blank sky region away from the source. These values are listed in Table 2, and the distribution of extended flux density values is shown in Figure 2.

The images of several sources (0202+149, 0212+735, 0552+398, 0642+449, 1324+224, 1417+385 and 2209+238) required futher analysis to confirm the presence of very faint extended emission. The core component was subtracted from the data, and the residual image was inspected for emission above 3 times the r.m.s. noise level. This was found for all but two sources, 0642+449 and 2209+238. For these two sources we set an upper limit on extended emission equal to 3 times the r.m.s. noise. We cannot rule out the presence of low−level diffuse emission on larger angular scales than the restoring beam, however.

3. Discussion

The sources in the MOJAVE sample appear highly core−dominated, since they are selected on the basis of compact VLBA emission, and not total (single−dish) flux. Indeed, nearly half of the objects we have imaged have less than 50 mJy in extended emission at 1.4

[1]AIPS is copyrighted by Associated Universities, Inc. using the GNU copyright form.

[2]DIFMAP was written by Martin Shepard at Caltech, and is part of the Caltech VLBI software package.

Table 1. Log of VLA Observations

Observation Date (1)	Number of Sources Observed (2)	Flux Density Calibrator (3)	Number of VLA Antennas (4)
2004 Sep 19	21	0134+329 (3C 048)	24
2004 Nov 03	7	0134+329 (3C 048)	25
2004 Nov 09	9	0134+329 (3C 048)	25
2004 Nov 20	6	1328+307 (3C 286)	25
2004 Nov 21	12	0134+329 (3C 048)	24
2004 Nov 24	5	0538+498 (3C 147)	24

GHz. In Figure 3 we show a histogram of the logarithm of core−to−extended luminosity ratio (R_c). These values were K−corrected to the rest frame of each AGN using redshifts from the NASA Extragalactic Database assuming spectral indices of $\alpha = 0$ and $\alpha = -0.7$ $(S \propto \nu^{\alpha})$ for the core and extended emission respectively. For sources without redshift information, z = 1 was assumed. The shape of the distribution is similar to that found by a core−dominated AGN sample by Murphy et al. (1993), with a broad peak centered at $R_c \simeq 10$.

4. Conclusions

We have obtained high−dynamic range VLA−A configuration images at 1.4 GHz of 57 AGN in the MOJAVE sample as part of a project to investigate a possible correlation between extended jet luminosity of blazars and parsec−scale jet speed. We found extended emission above the ∼0.3 mJy level in all but two sources. A more detailed analysis of the full MOJAVE sample, using arcsecond−scale radio images from previous studies, the VLA archive and other observations, will be presented in an upcoming paper.

The authors wish to acknowledge the contributions of the other members of the MOJAVE project team: Hugh and Margo Aller, Tigran Arshakian, Steve Bloom, Marshall Cohen, Dan Homan, Matthias Kadler, Ken Kellermann, Yuri Kovalev, Andrei Lobanov, Eduardo Ros, Rene Vermeulen, and Tony Zensus.

This research was supported by NSF grant 0406923-AST and made use of the following resources: The NASA/IPAC Extragalactic Database (NED), which is operated by the Jet Propulsion Laboratory, California Institute of Technology, under contract with the National Aeronautics and Space Administration. The Very Large Array (VLA), which is operated by The National Radio Astronomy Observatory (NRAO). The NRAO is a facility of the National Science foundation, operated under cooperative agreement with Associated Universities, INC.

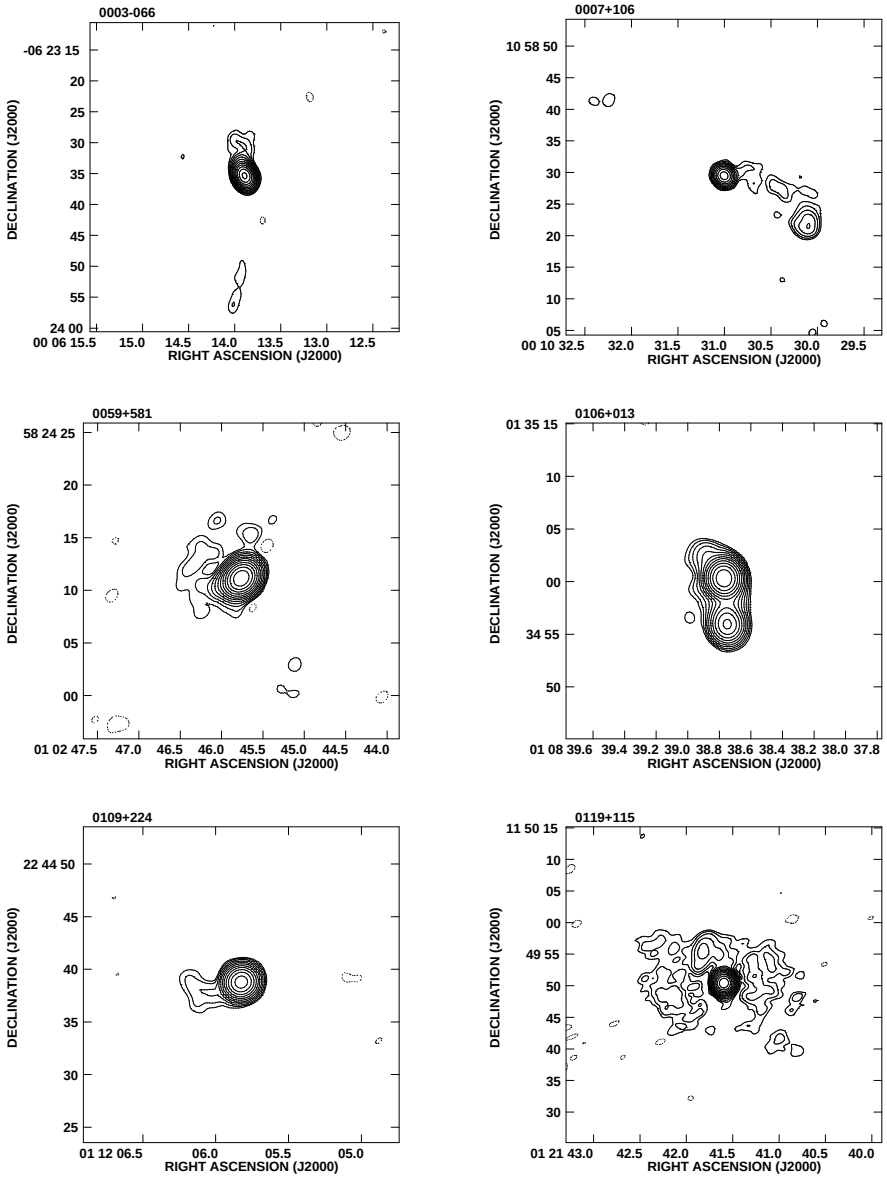

Fig. 1.— 1.4 GHz VLA−A configuration images of AGN in the MOJAVE sample. Each panel contains a Stokes I parameter image of the source, with contours in successive integer powers of two times the lowest contour (see Table 2). A single negative contour equal in magnitude to the lowest contour is indicated with dashed lines.

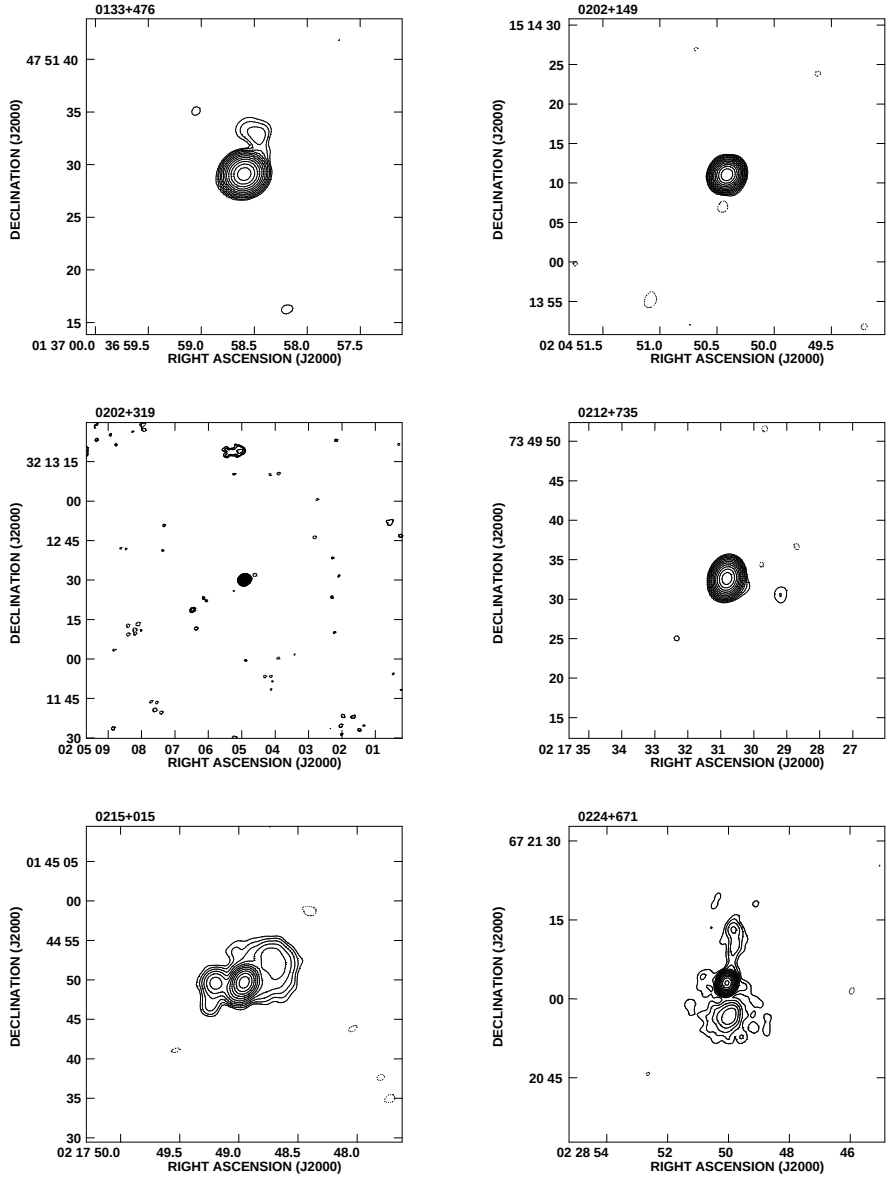

Fig. 1.— (continued)

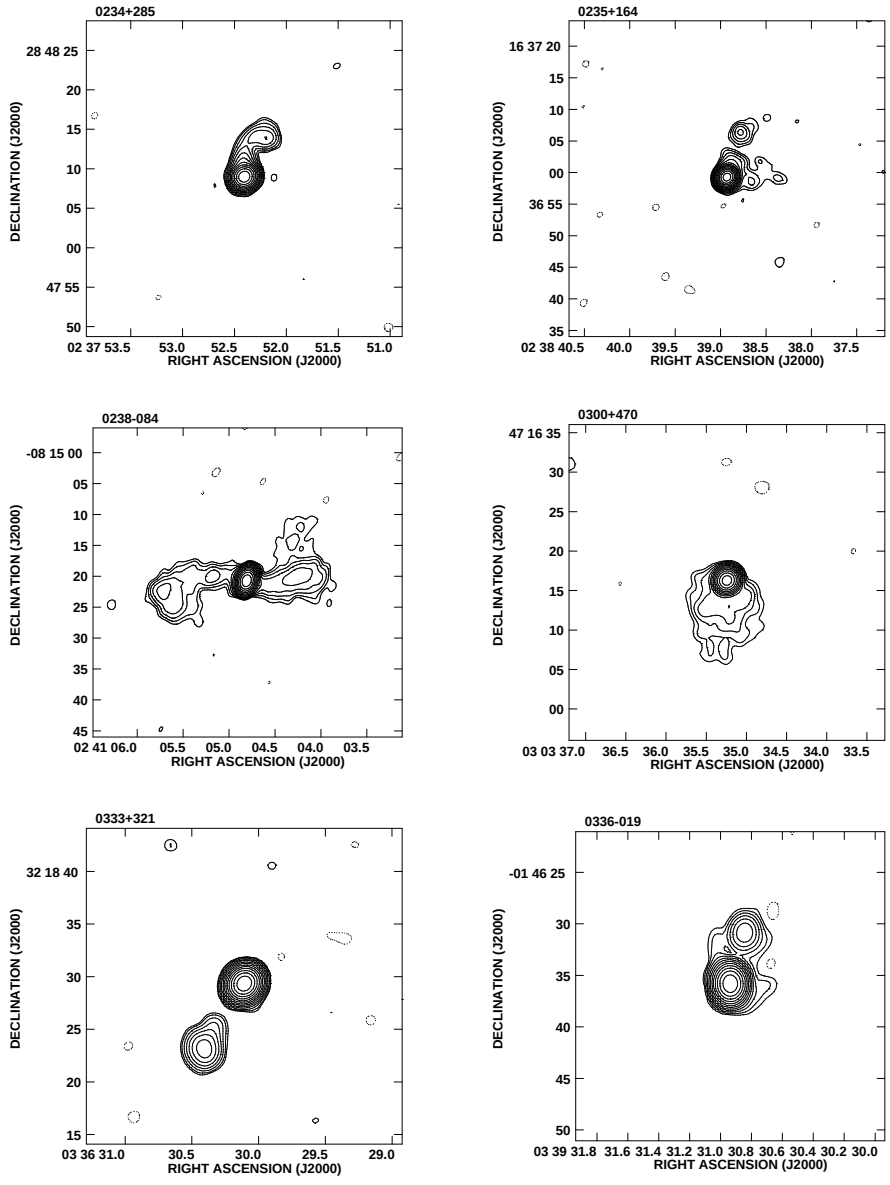

Fig. 1.— (continued)

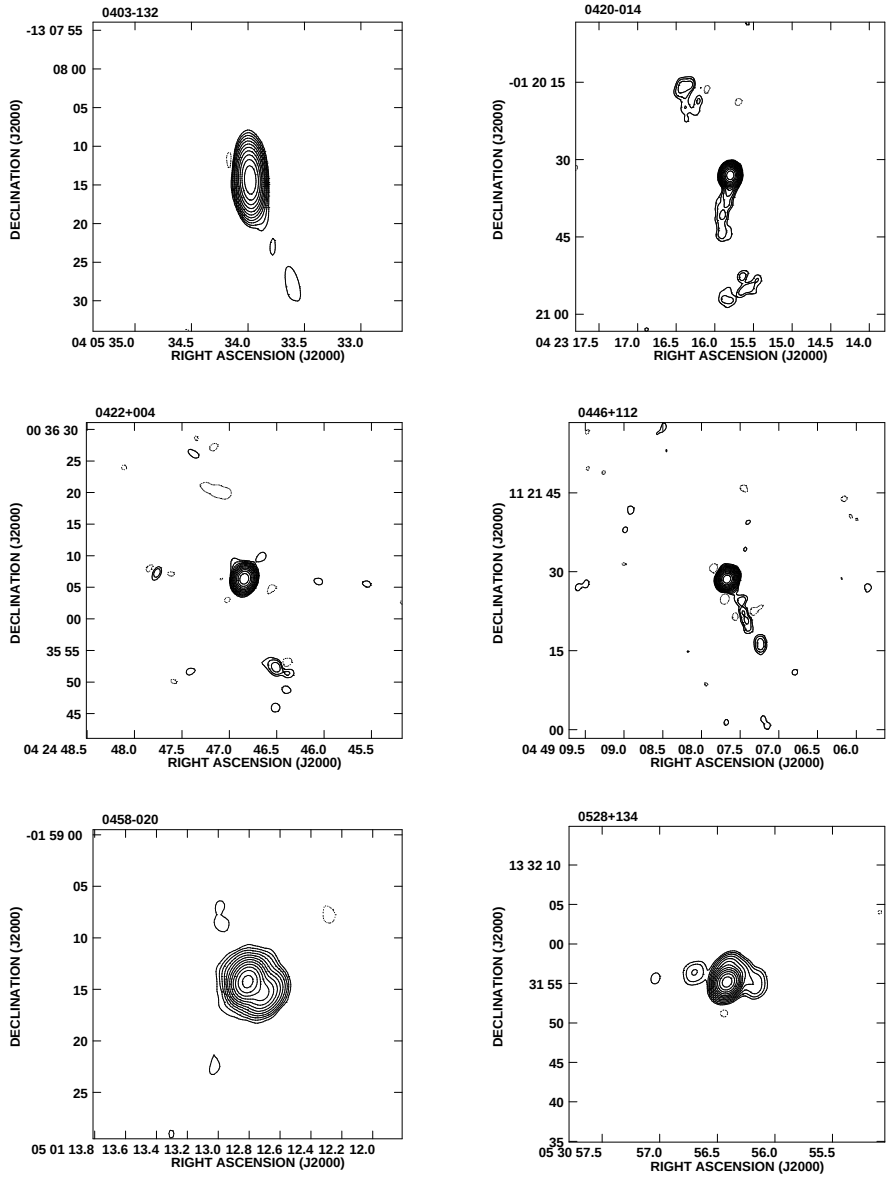

Fig. 1.— (continued)

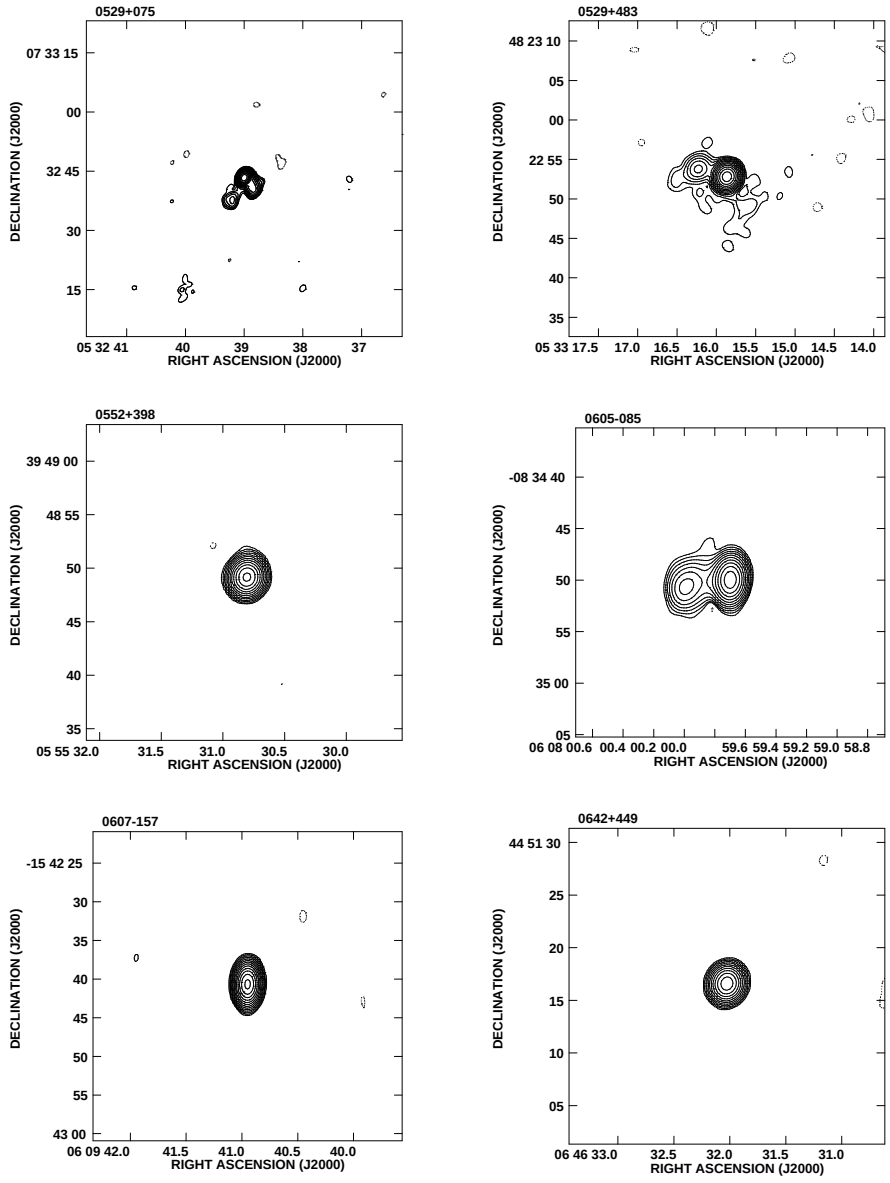

Fig. 1.— (continued)

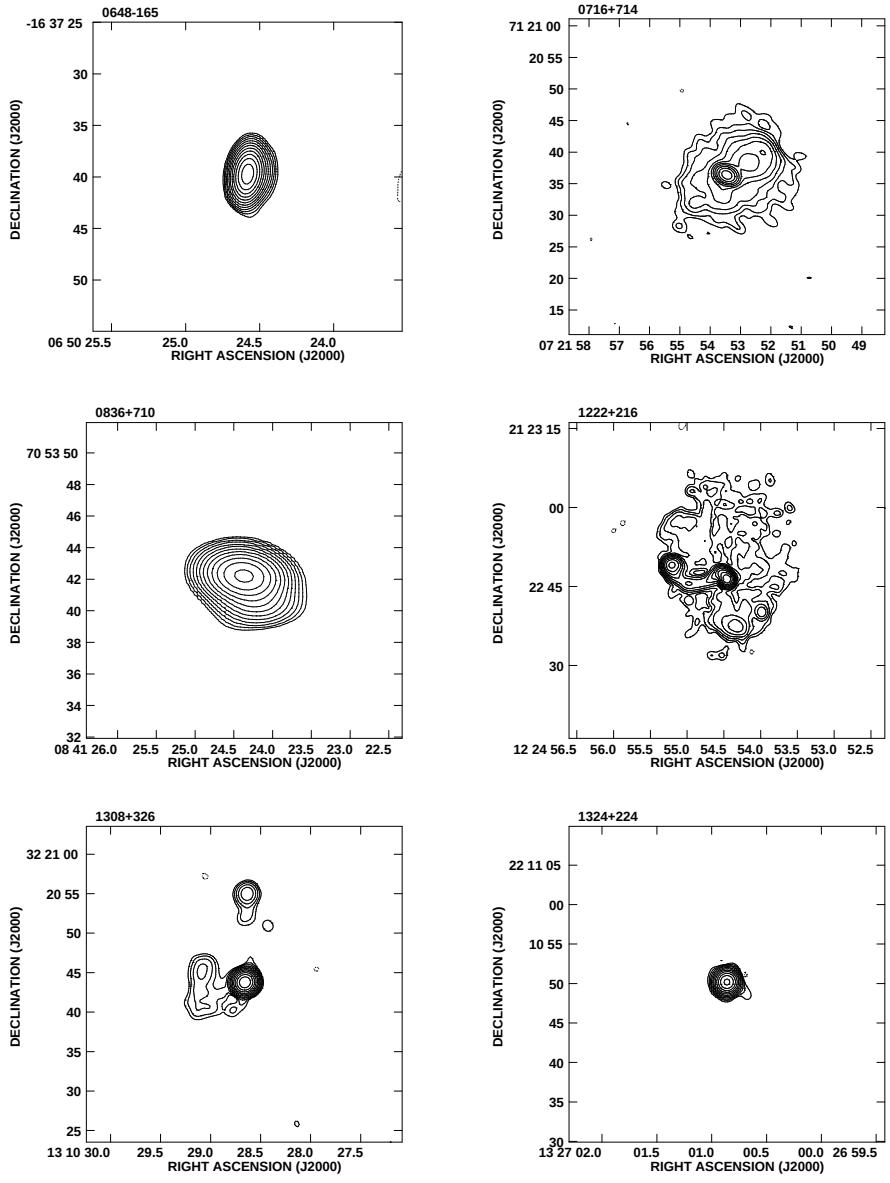

Fig. 1.— (continued)

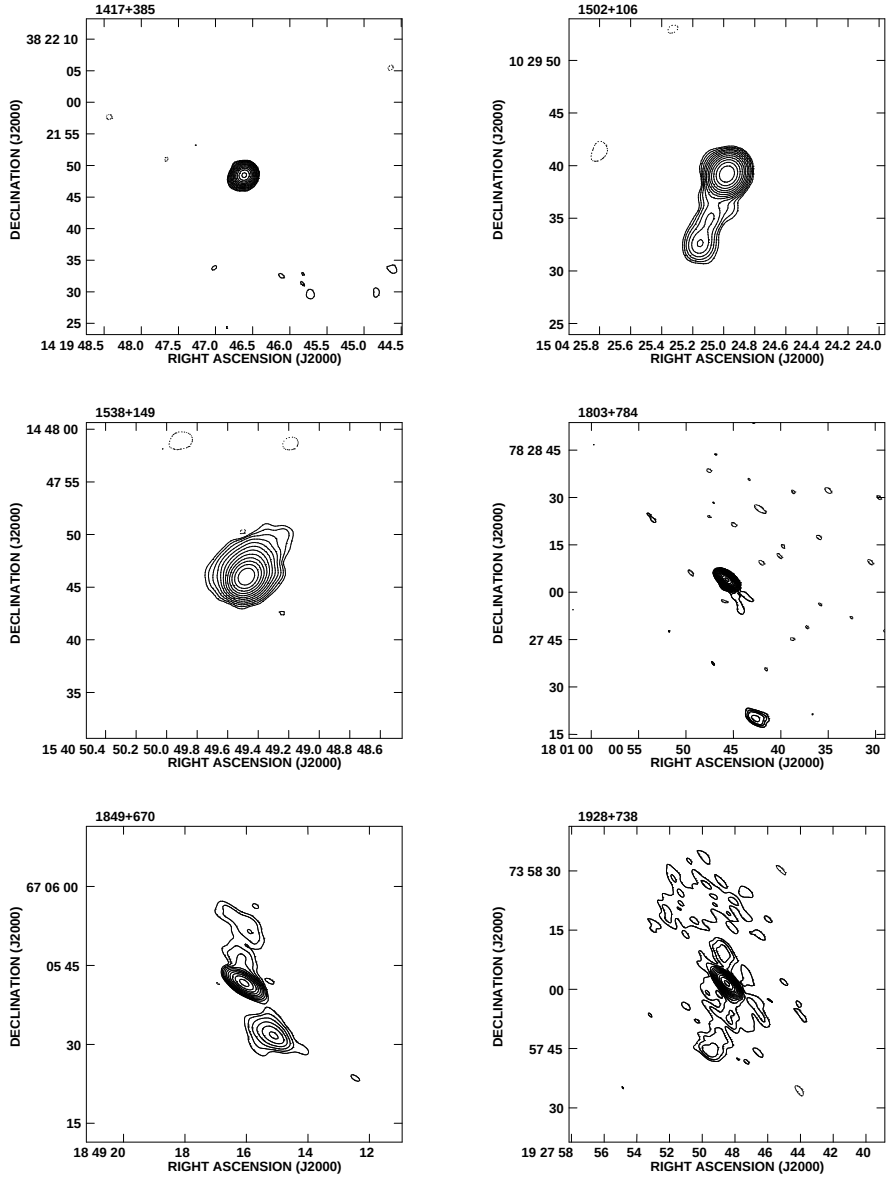

Fig. 1.— (continued)

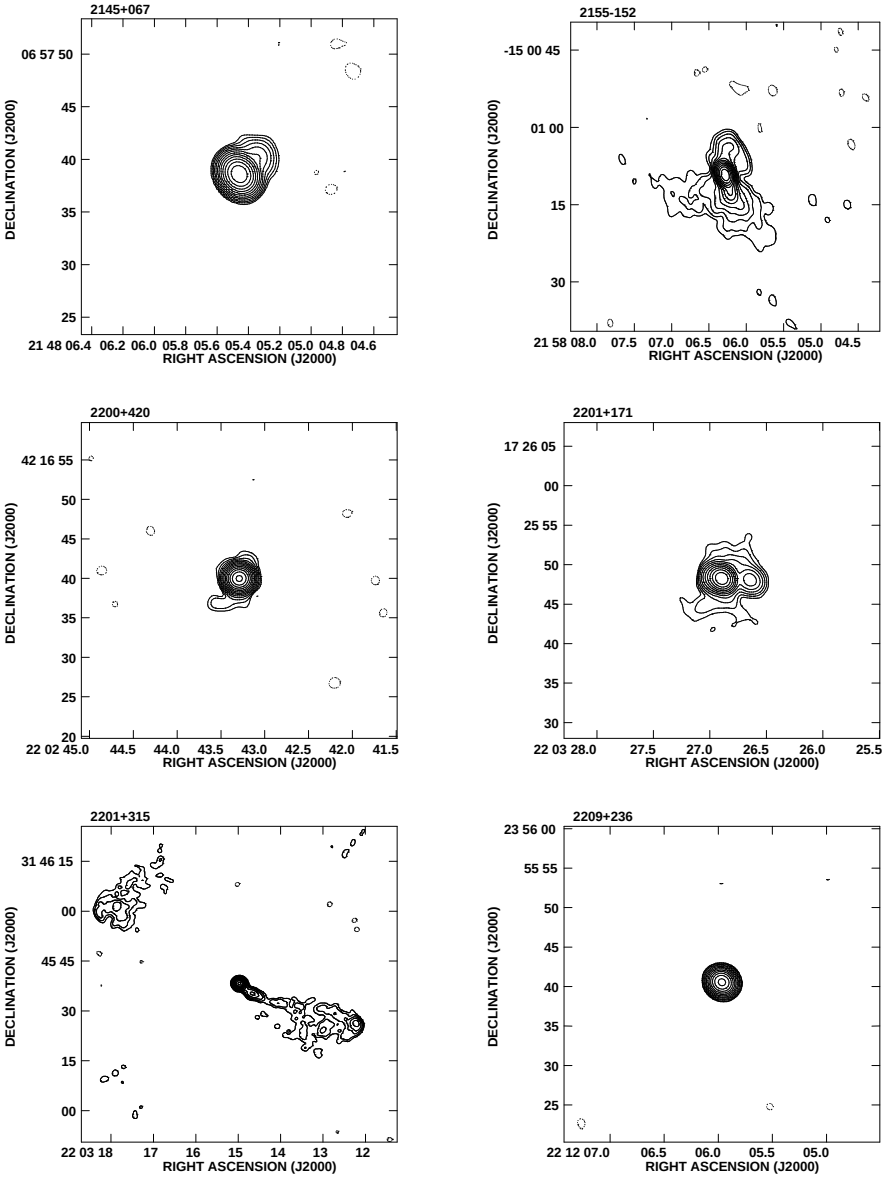

Fig. 1.— (continued)

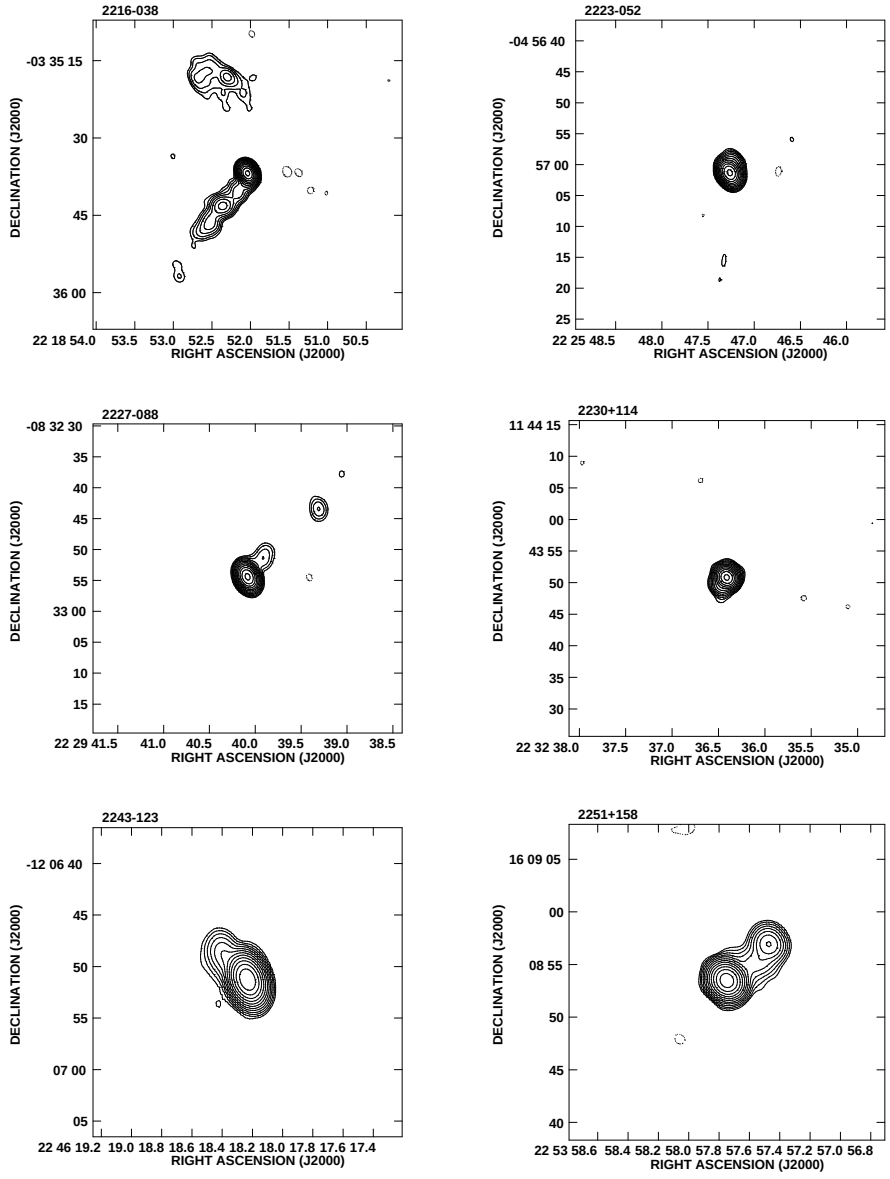

Fig. 1.— (continued)

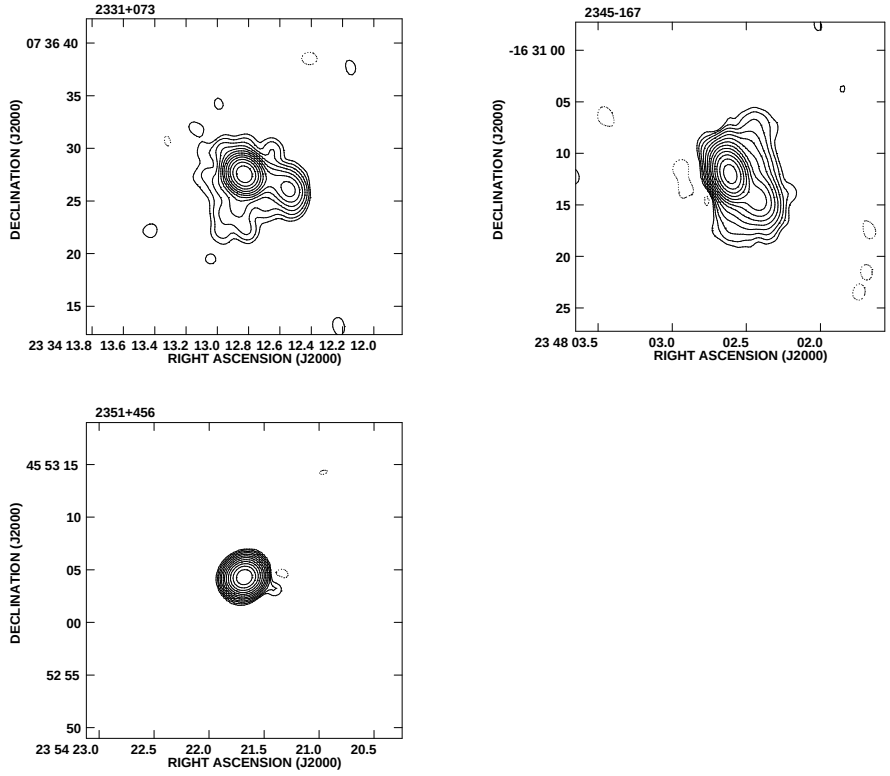

Fig. 1.— (continued)

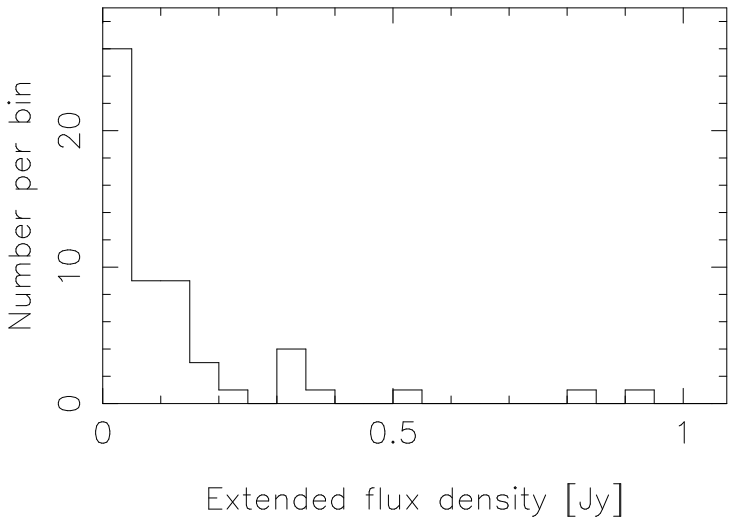

Fig. 2.— Distribution of 1.4 GHz extended flux density for 57 AGN in the MOJAVE sample.

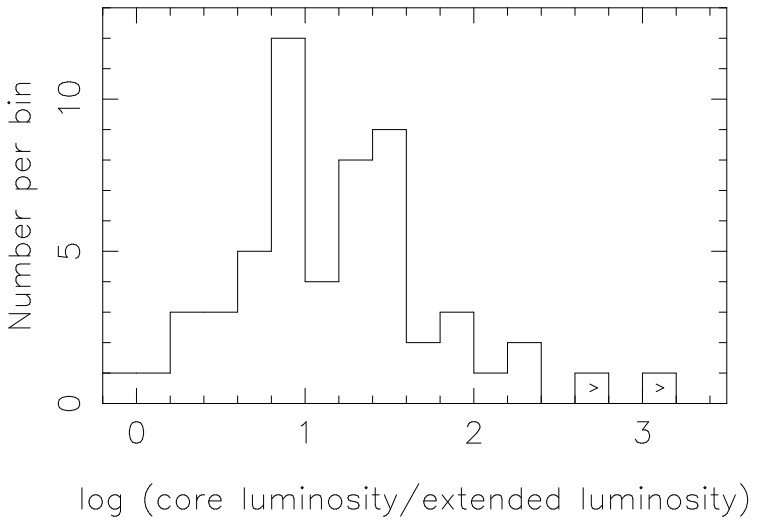

Fig. 3.— Distribution of core−to−extended luminosity ratio (source frame) for 57 AGN in the MOJAVE sample.

Table 2. Image and Source Properties at 1.4 GHz

Source	S_{core} (Jy)	S_{ext} (Jy)	R.M.S. (mJy beam^{-1})	Lowest Contour (mJy beam^{-1})	B_{maj} (arcsec)	B_{min} (arcsec)	B_{PA} (degrees)
(1)	(2)	(3)	(4)	(5)	(6)	(7)	(8)
0003−066	2.639	0.057	0.19	1.04	1.92	1.41	23.6
0007+106	0.077	0.016	0.04	0.38	1.62	1.46	43.6
0059+581	1.565	0.030	0.17	0.78	1.64	1.35	−45.1
0106+013	2.801	0.536	0.17	0.69	1.64	1.49	9.6
0109+224	0.361	0.006	0.08	0.45	1.49	1.42	−63.5
0119+115	1.230	0.125	0.10	0.59	1.53	1.44	−34.8
0133+476	1.874	0.016	0.12	0.56	1.55	1.41	−61.2
0202+149	3.840	0.016	0.17	0.95	1.58	1.42	−40.5
0202+319	0.650	0.012	0.13	0.52	1.55	1.37	−60.2
0212+735	2.461	0.010	0.12	0.74	1.83	1.44	−14.0
0215+015	0.446	0.074	0.08	0.50	1.74	1.43	−26.9
0224+671	1.484	0.151	0.11	0.59	1.69	1.42	−22.1
0234+285	2.313	0.119	0.10	1.14	1.47	1.35	−54.3
0235+164	1.507	0.034	0.07	0.45	1.51	1.38	−35.7
0238−084	1.111	0.111	0.08	0.27	1.95	1.43	−16.5
0300+470	1.175	0.062	0.08	0.35	1.47	1.41	−36.4
0333+321	3.008	0.080	0.12	0.75	1.50	1.36	−41.0
0336−019	2.907	0.088	0.24	0.73	1.74	1.44	2.2
0403−132	4.311	0.027	0.37	2.00	3.62	1.44	1.3
0420−014	2.889	0.087	0.11	0.72	1.72	1.41	−4.6
0422+004	1.078	0.014	0.14	1.08	1.71	1.40	−16.7
0446+112	1.543	0.032	0.17	0.38	1.57	1.38	−28.7
0458−020	1.068	0.134	0.09	0.70	1.78	1.41	−18.9
0528+134	2.230	0.074	0.14	0.66	1.62	1.36	−33.2
0529+075	1.551	0.118	0.12	0.76	1.70	1.35	−26.6
0529+438	0.649	0.023	0.09	0.39	1.50	1.36	−23.9
0552+398	1.539	0.009	0.15	0.61	1.50	1.34	−10.9
0605−085	1.209	0.116	0.17	0.70	1.99	1.37	−2.8
0607−157	3.009	0.014	0.20	0.60	2.27	1.36	−1.2
0642+449	0.645	<0.0003	0.09	0.39	1.50	1.34	−13.7
0648−165	2.109	0.028	0.15	0.63	2.34	1.34	−8.3
0716+714	0.715	0.347	0.07	0.39	2.00	1.46	61.7
0836+710	3.274	0.139	0.18	12.65	2.24	1.43	80.9
1222+216	1.115	0.943	0.08	0.47	1.45	1.41	24.4
1308+326	1.330	0.069	0.19	0.65	1.43	1.37	−46.2
1324+224	1.131	0.009	0.17	0.90	1.44	1.41	−15.0
1417+385	0.515	0.008	0.07	0.40	1.46	1.37	−42.4
1502+106	1.808	0.046	0.08	0.45	1.62	1.39	−30.3
1538+149	1.633	0.104	0.09	0.36	1.65	1.37	−41.1
1803+784	1.974	0.032	0.12	0.79	2.93	1.47	50.7
1849+670	0.475	0.101	0.13	0.70	3.39	1.50	55.9
1928+738	3.209	0.359	0.18	1.28	3.50	1.40	43.7
2145+067	2.853	0.040	0.17	0.71	1.73	1.45	35.4
2155−152	2.686	0.315	0.17	0.65	2.29	1.48	18.9

REFERENCES

Antonucci, R., & Ulvestad, J. 1985, ApJ, 294, 158

Blandford, R., Rees, M. 1974, MNRAS, 169, 395

Cassaro, P., 1999, A&AS, 139, 601

Cawthorne, T. V., Wardle, J. F. C., Roberts, D. H., & Gabuzda, D. C. 1993, ApJ, 416, 519

Cohen et al., 2007, ApJ, in press

Giovannini et al. 1988, A&A, 199, 73

Kato, Y., Mineshige, S., & Shibata, K. 2004, ApJ, 605, 307

Kellermann, K. I., Vermeulen, R. C., Zensus, J. A., Cohen, M. H. 1998, AJ, 115, 1295

Kellermann et al., 2004, ApJ, 609, 539

Lister, M. L. 2001, ApJ, 562, 208

Lister, M. L. & Homan D. C. 2005, AJ, 130, 1389

Lister, M. L. & Marscher, A. P. 1997, ApJ, 476, 572

Murphy, D., Browne, I., Perley, R. 1993, MNRAS, 264, 298

Perley, R. A. 1982, AJ, 87, 859

Rector, T. & Stocke, J. 2001, AJ, 122, 565

Table 2—Continued

Source	S_{core} (Jy)	S_{ext} (Jy)	R.M.S. (mJy beam^{-1})	Lowest Contour (mJy beam^{-1})	B_{maj} (arcsec)	B_{min} (arcsec)	B_{PA} (degrees)
(1)	(2)	(3)	(4)	(5)	(6)	(7)	(8)
2200+420	1.980	0.025	0.07	0.39	1.52	1.45	87.9
2201+171	0.867	0.082	0.06	0.41	1.63	1.44	49.9
2201+315	1.525	0.314	0.13	0.61	1.57	1.43	74.0
2209+236	0.426	<0.0002	0.07	0.32	1.57	1.43	58.7
2216−038	1.766	0.302	0.17	2.76	1.93	1.47	27.3
2223−052	7.057	0.153	0.30	2.69	1.94	1.45	26.3
2227−088	0.922	0.013	0.09	0.37	2.08	1.46	24.7
2230+114	6.891	0.246	0.44	2.63	1.70	1.46	39.8
2243−123	2.259	0.038	0.23	0.56	2.19	1.46	20.1
2251+158	14.075	0.836	0.44	4.14	1.65	1.44	37.7
2331+073	0.609	0.038	0.06	0.30	1.69	1.45	36.2
2345−167	1.981	0.152	0.08	0.57	2.27	1.45	17.8
2351+456	2.332	0.021	0.04	0.56	1.54	1.39	−65.5

Note. — Columns are as follows: (1) IAU Name (B1950.0); (2) Fitted Gaussian core flux density in Jy; (3) Extended flux density of the source in Jy; (4) R.M.S. noise of the image in mJy beam^{-1}; (5) Minimum contour level of the image in mJy beam^{-1}; (6) FWHM major axis of the restoring beam in arcseconds; (7) FWHM minor axis of the restoring beam in arcseconds; (8) Major axis position angle of the restoring beam in degrees.